Applied and Computational Harmonic Analysis **9**, 83–97 (2000)
doi:10.1006/acha.2000.0310, available online at http://www.idealibrary.com on IDEAL®

CASE STUDY

Spectral Approximation of the Free-Space Heat Kernel

Leslie Greengard [1,2] and Patrick Lin [1,3]

Communicated by Vladimir Rokhlin
Received September 3, 1999

Abstract—Many problems in applied mathematics, physics, and engineering require the solution of the heat equation in unbounded domains. Integral equation methods are particularly appropriate in this setting for several reasons: they are unconditionally stable, they are insensitive to the complexity of the geometry, and they do not require the artificial truncation of the computational domain as do finite difference and finite element techniques. Methods of this type, however, have not become widespread due to the high cost of evaluating heat potentials. When m points are used in the discretization of the initial data, M points are used in the discretization of the boundary, and N time steps are computed, an amount of work of the order $O(N^2M^2 + NMm)$ has traditionally been required. In this paper, we present an algorithm which requires an amount of work of the order $O(NM \log M + m \log m)$ and which is based on the evolution of the *continuous* spectrum of the solution. The method generalizes an earlier technique developed by Greengard and Strain (1990, *Comm. Pure Appl. Math.* **43**, 949) for evaluating layer potentials in bounded domains.

1. INTRODUCTION

The numerical solution of the heat equation

$$U_t = \Delta U$$

arises as a computational task in heat transfer, solidification, fluid dynamics, finance, and a variety of other areas of applied mathematics. In some cases, one wants to solve the pure

[1] Courant Institute of Mathematical Sciences, New York University, New York, New York 10012.

[2] The work of this author was supported by the Applied Mathematical Science Program of the U.S. Department of Energy under Contract DEFGO288ER25053, by a NSF Presidential Young Investigator Award, and by a Packard Foundation Fellowship.

[3] The work of this author was supported by a NSF Presidential Young Investigator Award to Leslie Greengard and by the Office of Naval Research Grant N00014-91-J-1312. Present address: Municipal Derivatives, Citibank, 399 Park Ave., 7th Floor, New York, NY 10043.

1063-5203/00 $35.00

initial value problem

$$\begin{aligned} U_t(\mathbf{x},t) &= \Delta U(\mathbf{x},t) \qquad \text{for } t>0 \\ U(\mathbf{x},0) &= f(\mathbf{x}) \qquad \text{for } \mathbf{x}\in\mathbf{R}^d, \end{aligned} \tag{1}$$

while in other cases, one is given initial and boundary data on an *interior* or *exterior* space–time domain $\Omega_T = \prod_{t=0}^{T}\Omega(t)$ with boundary $\Gamma_T = \prod_{t=0}^{T}\Gamma(t)$, where $\Gamma(t) = \partial\Omega(t)$. (When the spatial domain is not time-dependent, we can write, more simply, $\Omega_T = \Omega\times[0,T]$ and $\Gamma_T = \Gamma\times[0,T]$.)

There are many possible approaches to such problems, the most common of which are finite difference and finite element methods, which we do not seek to review here. Rather, we are interested in continuing the examination of integral equation methods begun in [10, 11]. The first of these papers describes an algorithm for solving the pure initial value problem (1), i.e., evaluating integrals of the form

$$U(\mathbf{x},t) = (4\pi t)^{-d/2}\int_{\mathbf{R}^d} e^{-|\mathbf{x}-\mathbf{y}|^2/4t} f(\mathbf{y})\,d\mathbf{y}.$$

This *fast Gauss transform* requires $O(n+m)$ work to determine $U(\mathbf{x},t)$ at n points given the initial data $f(\mathbf{y})$ at m points. The second paper describes a rather different algorithm for rapidly evaluating layer heat potentials, with application to solving the heat equation on arbitrary but bounded domains. In the present paper, we study the remaining case, namely the solution of initial–boundary value problems in exterior regions, where the spectrum is continuous and the Fourier series approach of [11] does not apply (or, more precisely, is inefficient). For a complementary approach, related to the fast Gauss transform, we refer the reader to the recent algorithm of Strain [23].

Consider now, as a typical example, the Dirichlet problem in an exterior time-dependent domain $\Omega(t)\in\mathbf{R}^d$ with known boundary $\Gamma(t)$,

$$U_t = \Delta U \qquad \text{in } \Omega(t) \tag{2}$$

$$U(\mathbf{x},t) = f(\mathbf{x}) \qquad \text{in } \Omega(0) \tag{3}$$

$$U(\mathbf{x},t) = g(\mathbf{x},t) \qquad \text{on } \Gamma(t). \tag{4}$$

Classical potential theory [9, 12, 20] suggests that we seek a solution U of the form

$$U(\mathbf{x},t) = \int_{\Omega(0)} G(\mathbf{x}-\mathbf{y},t) f(\mathbf{y})\,d\mathbf{y} + \int_0^t\int_{\Gamma(\tau)} \frac{\partial}{\partial\nu_{\mathbf{y}}} G(\mathbf{x}-\mathbf{y},t-\tau)\mu(\mathbf{y},\tau)\,d\mathbf{y}\,d\tau, \tag{5}$$

where G is the fundamental solution of the heat equation in free space

$$G(\mathbf{x},t) = (4\pi t)^{-d/2}\exp\left(-\frac{\|\mathbf{x}\|^2}{4t}\right),$$

$\nu_{\mathbf{y}}$ is the unit outward normal to $\Gamma(t)$ at $\mathbf{y}$, and μ is an unknown surface density defined on $\Gamma(t)$. We will refer to the first integral in (5) as an *initial potential*, denoted by Vf, and the second integral in (5) as a *double layer potential*, denoted by $D\mu$. This representation of U clearly satisfies (2) and (3). It remains only to satisfy (4). Allowing $\mathbf{x}$ to approach the boundary $\Gamma(t)$ and using the standard jump relations for a double layer potential [9, 12, 20], we obtain a Volterra integral equation for the density μ,

$$\frac{1}{2}\mu(\mathbf{x},t) - \int_0^t \int_{\Gamma(\tau)} \frac{\partial}{\partial \nu_{\mathbf{y}}} G(\mathbf{x}-\mathbf{y}, t-\tau)\mu(\mathbf{y},\tau)\, d\mathbf{y}\, d\tau$$
$$= \int_{\Omega(0)} G(\mathbf{x}-\mathbf{y}, t) f(\mathbf{y})\, d\mathbf{y} - g(\mathbf{x},t), \qquad \mathbf{x} \in \Gamma(t). \tag{6}$$

Using the more concise operator notation, we can write the preceding equation in the form

$$\frac{1}{2}\mu(\mathbf{x},t) - D\mu(\mathbf{x},t) = Vf(\mathbf{x},t) - g(\mathbf{x},t). \tag{7}$$

Some numerical work based on direct discretization of equations like (6) has been described in both the mathematical literature [16, 19] and the engineering literature. The latter is fairly extensive, so we simply refer the reader to the monographs [4, 18]. Nevertheless, the use of such methods has received only specialized interest due to the enormous attendant cost. Both Eq. (6) and the representation (5) are fully history dependent. Just to evaluate U on the space–time boundary $\Gamma(t)$, $0 < t \le T$, requires $O(N^2M^2 + NM \cdot m)$ work, where N is the number of time steps, M is the number of discretization points on the boundary, and m is the number of grid points used to represent the initial data. By contrast, the algorithm of [11], although limited to bounded domains, requires only $O(NM + m \log m)$ work. It has been used for large scale calculations of crystal growth by Sethian and Strain [21] and, in a modified version, by Brattkus and Meiron [3].

It is worth making a simple analytical observation at this point. We begin by letting δ be a small positive parameter and write the double layer potential $D\mu$ as the sum a *history* part, representing the influence of the density μ at distant times, and a *local* part, reflecting the influence of the density μ over the most recent time,

$$D\mu(\mathbf{x},t) = D_H\mu(\mathbf{x},t,\delta) + D_L\mu(\mathbf{x},t,\delta),$$

where

$$D_H\mu(\mathbf{x},t,\delta) = \int_0^{t-\delta} \int_{\Gamma(\tau)} \frac{\partial}{\partial \nu_{\mathbf{y}}} G(\mathbf{x}-\mathbf{y}, t-\tau)\mu(\mathbf{y},\tau)\, d\mathbf{y}\, d\tau \tag{8}$$

and

$$D_L\mu(\mathbf{x},t,\delta) = \int_{t-\delta}^{t} \int_{\Gamma(\tau)} \frac{\partial}{\partial \nu_{\mathbf{y}}} G(\mathbf{x}-\mathbf{y}, t-\tau)\mu(\mathbf{y},\tau)\, d\mathbf{y}\, d\tau. \tag{9}$$

We also introduce the notation

$$U_H(\mathbf{x},t) = Vf(\mathbf{x},t) + D_H\mu(\mathbf{x},t) \qquad \text{and} \qquad U_L(\mathbf{x},t) = D_L\mu(\mathbf{x},t),$$

so that

$$U(\mathbf{x},t) = U_H(\mathbf{x},t) + U_L(\mathbf{x},t).$$

The integral equation (7) can be then be written in the suggestive form

$$\frac{1}{2}\mu(\mathbf{x},t) - D_L\mu(\mathbf{x},t) = U_H(\mathbf{x},t) - g(\mathbf{x},t). \tag{10}$$

Note that at the current time t, the right-hand side of Eq. (10) is already known. Furthermore, the operator $D_L\mu$ is small. More precisely, it is easy to show (see [12]) that

$$\|D\|_\infty = O(\sqrt{\delta}).$$

Thus, (10) is very close to being an *explicit* formula for the unknown value of the density μ as time proceeds. Four steps of fixed point iteration, for example, would yield second order accuracy in δ. The point we wish to emphasize is that the evaluation of the history part U_H dominates the cost of both the solution of the integral equation (10) and the computation of the function U itself. The evaluation of the local part $D_L\mu$ can be accomplished through asymptotic methods, as in [11, 14] or through more accurate quadrature approaches, as in [22].

In this paper, we introduce a new algorithm for the rapid evaluation of the history part U_H which is closely related to the earlier "box" method of Greengard and Strain [11]. There, the kernel $K(\mathbf{x}, \mathbf{y}, t)$ used in the corresponding potentials is a Green's function for a box (a d-dimensional interval) which has a dual representation: one as an image system and one as a Fourier series. The basis for the algorithm is that U_H is smooth and well approximated using a small number of Fourier modes, while U_L is sharply peaked but well approximated by a series expansion in the parameter δ.

In exterior domains, however, the situation is more complex. The free-space heat kernel has a continuous spectrum and U_H is well represented, not by a small number of Fourier modes, but by a finite range of integration in Fourier space. The issue becomes one of quadrature; can one compute the Fourier integral efficiently? It turns out that one can, inexpensively and with high order accuracy, but not by using a uniform sampling. In fact, the central result of this paper is the observation that one can select a nearly optimal set of quadrature points and obtain rigorous error bounds for the resulting quadrature rule. This analysis is carried out in the next section, while Section 3 contains a description of the fast algorithm itself. We discuss future directions for research in Section 4.

2. SPECTRAL APPROXIMATION OF THE HEAT KERNEL

We begin by considering the heat kernel on an interval $[-a\pi, a\pi]$ with periodic boundary conditions. A Fourier series calculation shows that

$$K(x,t) = \frac{1}{2\pi a} \sum_{k=-\infty}^{\infty} e^{-k^2 t/a^2} e^{ikx/a}, \tag{11}$$

while the method of images shows that

$$K(x,t) = \frac{1}{\sqrt{4\pi t}} \sum_{k=-\infty}^{\infty} e^{-(x-2\pi ak)^2/4t}. \tag{12}$$

The equivalence of the two representations is a particular instance of the Poisson summation formula [8]. For $t \geq \delta > 0$, truncation of the Fourier series after p terms yields

an error

$$E_p^F \equiv K(x,t) - \frac{1}{2\pi a}\sum_{k=-p}^{p} e^{-k^2 t/a^2} e^{ikx/a},$$

which is easily seen to satisfy the estimate

$$|E_p^F| \le \frac{1}{\sqrt{4\pi\delta}} e^{-p^2\delta/a^2}. \tag{13}$$

Letting $a \to \infty$ in (11) and (12), we obtain the integral formula

$$G(x,t) = \frac{e^{-x^2/4t}}{\sqrt{4\pi t}} = \frac{1}{2\pi}\int_{-\infty}^{\infty} e^{-s^2 t} e^{isx}\, ds. \tag{14}$$

Consider now the use of the trapezoidal rule with mesh spacing $1/a$ to approximate the integral in (14). Simple inspection shows that one recovers the Fourier series (11). This cannot be a valid approximation of the free-space heat kernel, at least for long times, unless $a \to \infty$. In physical terms, the problem is that for a given mesh spacing $1/a$, there are image sources at $x - 2\pi a$, $x + 2\pi a$, $x - 4\pi a$, $x + 4\pi a$, ..., in accordance with the representation (12). These source will pollute the solution as $t \to \infty$. By letting $a \to \infty$, we push these spurious sources farther and farther away. Unfortunately, the estimate (13) then shows that the number of retained Fourier modes must go to infinity as well.

To understand why the Fourier series fails as an approximation, it should first be noted that the issue is not one of aliasing in the usual sense. High frequency information, as one would expect, is rapidly damped and can be reliably ignored. The analog of the estimate (13) is provided by the following lemma, whose proof is straightforward.

LEMMA 2.1. *For $t \ge \delta > 0$,*

$$\left| \frac{e^{-x^2/4t}}{\sqrt{4\pi t}} - \frac{1}{2\pi}\int_{-p}^{p} e^{-s^2 t} e^{isx}\, ds \right| \le \frac{e^{-p^2\delta}}{\sqrt{4\pi\delta}}.$$

The essential difficulty is easily illustrated by means of a simple example. In Fig. 1, we plot the solution to the equation

$$U_t = U_{xx}, \qquad t \ge 0 \tag{15}$$

$$U(x,0) = \delta(x) \tag{16}$$

as well as its Fourier transform at times $t = 0.02, 1, 100$. Clearly, the problem with the Fourier series is that excessively dense sampling is required to correctly resolve the *lowest* frequency information. We must, therefore, abandon the trapezoidal rule and, along with it, the classical fast Fourier transform (FFT). Mathematically (and numerically), the relevant question is this: how many quadrature points are required on an interval $[a, b]$ in the Fourier domain in order to resolve the spectrum to within some specified precision ϵ? One answer is provided by the following theorem.

THEOREM 2.1. *Let $[a, b]$ be a dyadic interval of the form $[2^j, 2^{j+1}]$, let $t \ge \delta > 0$, let $\epsilon > 0$ be the desired precision, and let p be chosen so that*

$$\frac{1}{\sqrt{7\pi\delta}} e^{-p^2\delta} = \epsilon. \tag{17}$$

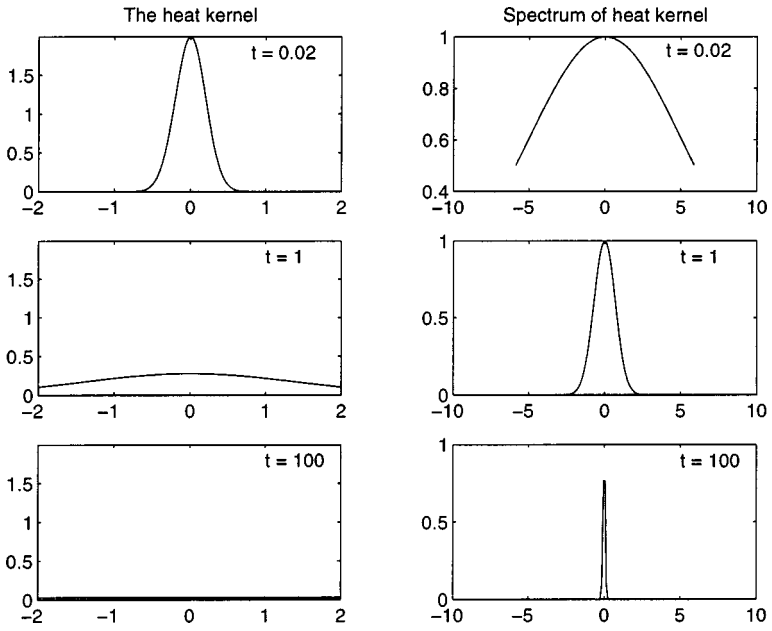

FIG. 1. The heat kernel in physical and Fourier space at $t = 0.02$, $t = 1.0$, and $t = 100$.

Finally, let $\{s_1, \ldots, s_n\}$ *and* $\{w_1, \ldots, w_n\}$ *be the nodes and weights for* n*-point Gauss–Legendre quadrature on the interval. Then, for dyadic intervals with* $j < 0$*, we have*

$$\left| \int_a^b e^{isx} e^{-s^2 t}\, ds - \sum_{k=1}^{n} e^{is_k x} e^{-s_k^2 t} w_k \right| \leq \sqrt{2\pi} \frac{(b-a)}{\sqrt{n}} \left[\frac{R(b-a)}{2n} + \sqrt{\frac{\log(1/\epsilon)}{n}} \right]^{2n} + (b-a)\epsilon \tag{18}$$

for $|x| \leq R$*. For dyadic intervals with* $j \geq 0$*, we have*

$$\left| \int_a^b e^{isx} e^{-s^2 t}\, ds - \sum_{k=1}^{n} e^{is_k x} e^{-s_k^2 t} w_k \right| \leq \sqrt{2\pi} \frac{(b-a)}{\sqrt{n}} \left[\frac{R(b-a)}{2n} + \sqrt{\frac{\log(1/\epsilon\sqrt{\delta})}{n}} \right]^{2n} + \frac{(b-a)\epsilon}{p} \tag{19}$$

for $|x| \leq R$*.*

Proof. For any interval $[a, b]$, the standard estimate for n-point Gauss–Legendre quadrature [6] yields

$$\left| \int_a^b e^{isx} e^{-s^2 t}\, ds - \sum_{k=1}^{n} e^{is_k x} e^{-s_k^2 t} w_k \right| \leq \frac{(b-a)^{2n+1}}{2n+1} \frac{(n!)^4}{(2n)!^3} \left| D_s^{2n} (e^{isx} e^{-s^2 t}) \right|_\infty, \tag{20}$$

where D_s denotes the partial derivative with respect to s.

Observe now that

$$D_s^j e^{isx} \leq R^j \qquad \text{for } |x| \leq R \tag{21}$$

and

$$D_s^j e^{-s^2 t} = (\sqrt{t})^j D_x^j e^{-x^2} = (\sqrt{t})^j h_j(x) \le \sqrt{2}(\sqrt{2t})^j(\sqrt{j!}), \tag{22}$$

where $h_j(x)$ is the classical Hermite function which satisfies Cramer's inequality [13]:

$$|h_j(x)| \le 2^{(j+1)/2}\sqrt{j!}.$$

Combining the last two results, we have

$$\begin{aligned} |D_s^n e^{isx} e^{-s^2 t}| &\le \sum_{j=0}^{n} \binom{n}{j} D_s^{n-j} e^{isx} D_s^j e^{-s^2 t} \\ &\le \sqrt{2} \sum_{j=0}^{n} \binom{n}{j} R^{n-j} (\sqrt{2t})^j \sqrt{j!} \\ &\le \sqrt{2} \sum_{j=0}^{n} \binom{n}{j} R^{n-j} (\sqrt{2tn})^j \le \sqrt{2}(R + \sqrt{2tn})^n. \end{aligned} \tag{23}$$

Inserting (23) into (20) and using Stirling's approximation [1]

$$\sqrt{2\pi} n^{n+1/2} e^{-n} < n! < 2\sqrt{\pi} n^{n+1/2} e^{-n},$$

it is easy to see that

$$\begin{aligned} &\left| \int_a^b e^{isx} e^{-s^2 t}\, ds - \sum_{k=1}^{n} e^{is_k x} e^{-s_k^2 t} w_k \right| \\ &\quad \le \sqrt{2\pi} \frac{(b-a)}{\sqrt{n}} \left[\frac{R(b-a)}{2n} + \frac{(b-a)\sqrt{t}}{\sqrt{2n}} \right]^{2n}. \end{aligned} \tag{24}$$

At first glance, this estimate appears useless, since the second term within the square brackets is unbounded in time. If $[a, b] = [2^j, 2^{j+1}]$ is a dyadic interval, however, then it is separated from the origin by its length. For small intervals ($j < 0$), once $(b-a)^2 t > \log(1/\epsilon)$, then $e^{-(b-a)^2 t} = e^{-a^2 t} < \epsilon$ and

$$\int_a^b e^{isx} e^{-s^2 t} ds < (b-a)\epsilon.$$

Thus, the estimate (24) need only be invoked for $(b-a)\sqrt{t} < \sqrt{\log(1/\epsilon)}$, and the result (18) follows. For large dyadic intervals ($j \ge 0$), the requirement (17) implies that

$$p = \left(\frac{\log(1/\epsilon\sqrt{\delta})}{\delta} \right)^{1/2}.$$

Once $(b-a)^2 t > \log(1/\epsilon\sqrt{\delta})$, we have $e^{-(b-a)^2 t} = e^{-a^2 t} < \epsilon\sqrt{\delta}$. A simple calculation then shows that

$$\int_a^b e^{isx} e^{-s^2 t}\, ds < (b-a)\epsilon/p.$$

The estimate (24) need only be invoked, therefore, for $(b-a)\sqrt{t} < \sqrt{\log(1/\epsilon\sqrt{\delta})}$, and the result (19) follows. ■

Note that, in the estimates (18) and (19), both terms in square brackets must be small for the quadrature to be accurate. The first term requires that the number of nodes scale like the length of the interval, while the second term requires that there be at least a constant number of nodes on each interval, *no matter how small*. The first condition dominates on large dyadic intervals, but the second dominates on small intervals near the origin, forcing discretization points to cluster exponentially at zero.

Remark 2.1. The preceding theorem does not apply to the intervals $[-2^{-j}, 0]$ or $[0, 2^{-j}]$. For any finite time t, however, it is easy to use the estimate (24) to establish that setting $j = 2 + \log_2 \sqrt{t}$ and $n = O(\log 1/\epsilon)$ guarantees that the quadrature error is of the order $O(\epsilon)$. To obtain a quadrature which is valid as $t \to \infty$, on the other hand, one needs to continue the refinement process until $j = \log(1/\epsilon) + 1$. At that point, $[-2^{-j}, 2^{-j}]$ is an ϵ-neighborhood of the origin and can be ignored.

We are now in a position to combine Lemma 2.1 with Theorem 2.1 to give a discrete spectral approximation of the heat kernel. The proof is straightforward.

COROLLARY 2.1 (Spectral resolution of the heat kernel). *Let $t \geq \delta > 0$, let $\epsilon > 0$ be the desired precision, let p be chosen according to* (17)*, let $L_{\min} = -\log(1/\epsilon)$, and let $L_{\max} = \lceil \log p \rceil$. Further, let $\{s_{j,1}, \ldots, s_{j,n(j)}\}$ and $\{w_{j,1}, \ldots, w_{j,n(j)}\}$ be the nodes and weights for $n(j)$-point Gauss–Legendre quadrature on the interval $[2^j, 2^{j+1}]$, where $n(j) = \max(R2^{j+1}, 4\log(1/\epsilon))$ for $j < 0$ and $n(j) = \max(R2^{j+1}, 4\log(1/\epsilon\sqrt{\delta}))$ for $j \geq 2$. Then*

$$\left| \frac{e^{-x^2/4t}}{\sqrt{4\pi t}} - \frac{1}{2\pi} \sum_{j=L_{\min}}^{L_{\max}} \sum_{k=1}^{n(j)} (e^{is_{j,k}x} + e^{-is_{j,k}x}) e^{-s_{j,k}^2 t} w_{j,k} \right| \leq 3\epsilon \tag{25}$$

for $|x| \leq R$.

Remark 2.2. The important fact which emerges from this theorem is that the total number of sampling points in frequency needed to approximate the heat kernel on the interval $[-a\pi, a\pi]$ with a precision ϵ is of the order $O(\log\epsilon + \pi ap)$. This should be compared with the Fourier series representation of the periodic heat kernel which requires precisely ap modes to obtain the same accuracy ϵ. In short, the preceding theorem shows that, for a fixed precision, the number of modes needed to resolve the free-space heat kernel is of the same order as the number needed to resolve the periodic heat kernel, despite the fact that one has a continuous spectrum and the other a discrete spectrum.

Remark 2.3. In the remainder of this paper, we let N_C denote the total number of nodes in the spectral approximation (25) and write

$$\frac{e^{-x^2/4t}}{\sqrt{4\pi t}} \approx \sum_{q=1}^{N_C} e^{is_q x} e^{-s_q^2 t} w_q. \tag{26}$$

TABLE 1
Number of Fourier Nodes Needed to Discretize the Free-Space Heat Kernel on $[-\pi, \pi]$ over Three Different Time Intervals: $I_1 = [0.001, 0.001]$, $I_2 = [0.001, 10]$, $I_3 = [0.001, \infty]$

ϵ	$p = s_{\max}$	$N_C(I_1)$	$N_F(I_1)$	$N_C(I_2)$	$N_F(I_2)$	$N_C(I_3)$	$N_F(I_3)$
10^{-4}	110	208	120	216	720	296	$\approx 10^5$
10^{-7}	140	282	160	294	1200	486	$\approx 10^8$
10^{-10}	165	332	184	368	1700	760	$\approx 10^{11}$
10^{-13}	185	478	220	502	2200	1100	$\approx 10^{14}$

Note. The first column indicates the desired precision ϵ. The second column indicates the maximum frequency p required for $t = \delta = 0.001$, according to Eq. (17). N_C denotes the number of composite Gaussian quadrature nodes using Corollary 2.1 and N_F denotes the number of Fourier modes needed by the trapezoidal rule (the standard Fourier series).

EXAMPLE 2.1. To verify the accuracy of our approximation and get a more concrete feeling for the number of spectral nodes needed in practice, we compute the free-space heat kernel

$$\frac{e^{-x^2/4t}}{\sqrt{4\pi t}}, \qquad -\pi \le x \le \pi,$$

from its spectral representation. In Table 1, the error is measured in the infinity norm by sampling at 100 points in the indicated range. We consider three cases: $0.001 \le t \le 0.001$, $0.001 \le t \le 10$, and $0.001 \le t \le \infty$. For the first two cases, we use the observation in Remark 2.1 to halt the dyadic refinement process once $2^{-j} \approx 1/4\sqrt{t}$.

As expected, for short times, the Fourier series approximation of the free-space heat kernel needs a number of nodes which only slightly exceeds p (the number of Fourier modes needed for representing the *periodic* heat kernel with precision ϵ). As the time interval increases, however, and image sources have the chance to diffuse in, the number of nodes grows like $\sqrt{t}$. The number of discrete spectral modes is bounded, of course, even as $t \to \infty$, because of the fact that we can ignore the heat kernel once it is below ϵ in the L_∞-norm. At $x = 0$, this occurs at $t \approx \epsilon^2$, which is a long time indeed. In Table 1, the number of nodes $N_C(I_3)$ is, in fact, determined by setting $t = \epsilon^{-2}$ and insisting that the specified error tolerance is met.

Remark 2.4. In Theorem 2.1, the number of modes chosen on each large dyadic interval is given by $n(j) = \max(R2^{j+1}, 4\log(1/\epsilon\sqrt{\delta}))$. Our estimates are not sharp, however. The data in Table 1, are obtained using a slight modification. On $[1, p]$, we use a single Gauss–Legendre grid with $C_0(p-1)$ nodes. For the first 10 dyadic refinements toward the origin, we use C_1 modes and for all subsequent dyadic refinements we use C_2 modes. For $\epsilon = 10^{-4}$, we set $C_0 = 0.9$, $C_1 = 4$, and $C_2 = 2$. For $\epsilon = 10^{-7}$, we set $C_0 = 0.95$, $C_1 = 6$, and $C_2 = 4$. For $\epsilon = 10^{-10}$, we set $C_0 = 1.0$, $C_1 = 8$, and $C_2 = 6$. Finally, for $\epsilon = 10^{-13}$, we set $C_0 = 1.2$, $C_1 = 12$, and $C_2 = 6$.

2.1. Higher Dimensional Approximation

We begin with the analog of Lemma 2.1, which bounds the error in truncating high frequency modes. The proof is elementary.

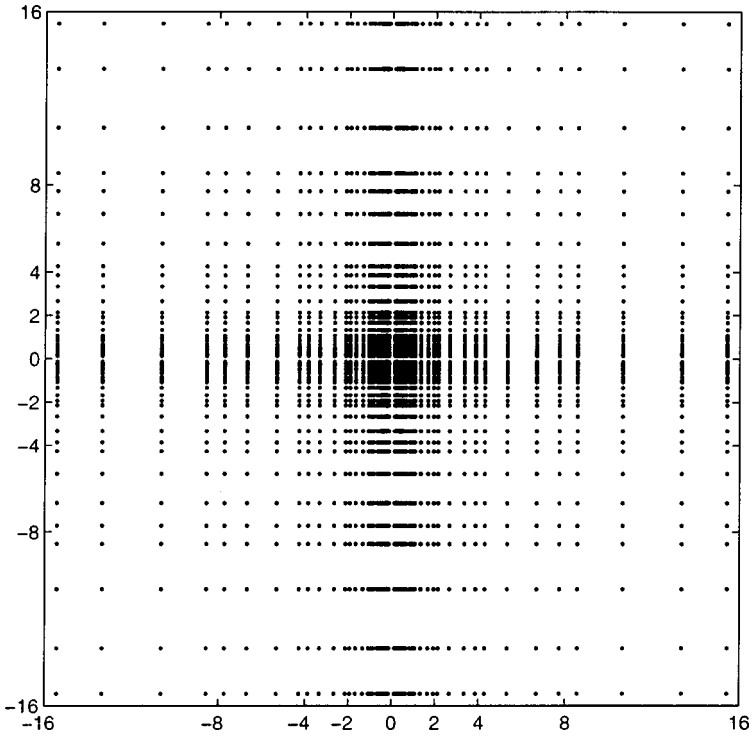

FIG. 2. Sampling nodes in the frequency domain representation of the two-dimensional heat kernel, using a tensor product discretization.

LEMMA 2.2. *For $t \geq \delta > 0$, $\mathbf{x}, \mathbf{s} \in \mathbf{R}^d$, we have*

$$\left| \frac{e^{-\|\mathbf{x}\|^2/4t}}{4\pi t} - \left(\frac{1}{2\pi}\right)^2 \int_{\|\mathbf{s}\| \leq p} e^{-\|\mathbf{s}\|^2 t} e^{i\mathbf{s}\cdot\mathbf{x}} \, d\mathbf{s} \right| \leq \frac{e^{-p^2\delta}}{8\pi^2\delta} \cdot \begin{cases} 2\pi & \text{for } d = 2 \\ \sqrt{\pi/\delta} + 2p & \text{for } d = 3. \end{cases}$$

The most natural discretization of the Fourier domain would use a radial grid, clustering exponentially at the origin. For the sake of simplicity, we will work with tensor product discretizations (Fig. 2) using the one-dimensional quadrature and omit the tedious analysis of the corresponding errors. To demonstrate that tensor product discretization is effective, however, we consider a concrete example.

EXAMPLE 2.2. Let

$$U(\mathbf{x}, t) = \frac{e^{-\|\mathbf{x}-\mathbf{y}_1\|^2/4t}}{4\pi t} + \frac{e^{-\|\mathbf{x}-\mathbf{y}_2\|^2/4t}}{4\pi t},$$

where $\mathbf{y}_1 = (-0.5, -0.5)$ and $\mathbf{y}_2 = (0.5, 0.5)$, with $0.005 < t < 50$. In Fig. 3, we plot the exact solution and three spectral approximations to $U(\mathbf{x}, t)$ at $t = 0.005$ using either the equispaced trapezoidal rule (a Fourier series) or a tensor product composite rule based on (26). Note that with too few Fourier modes, the image sources are clearly visible. In Fig. 4, we plot the exact solution and three spectral approximations to $U(\mathbf{x}, t)$ at $t = 50$.

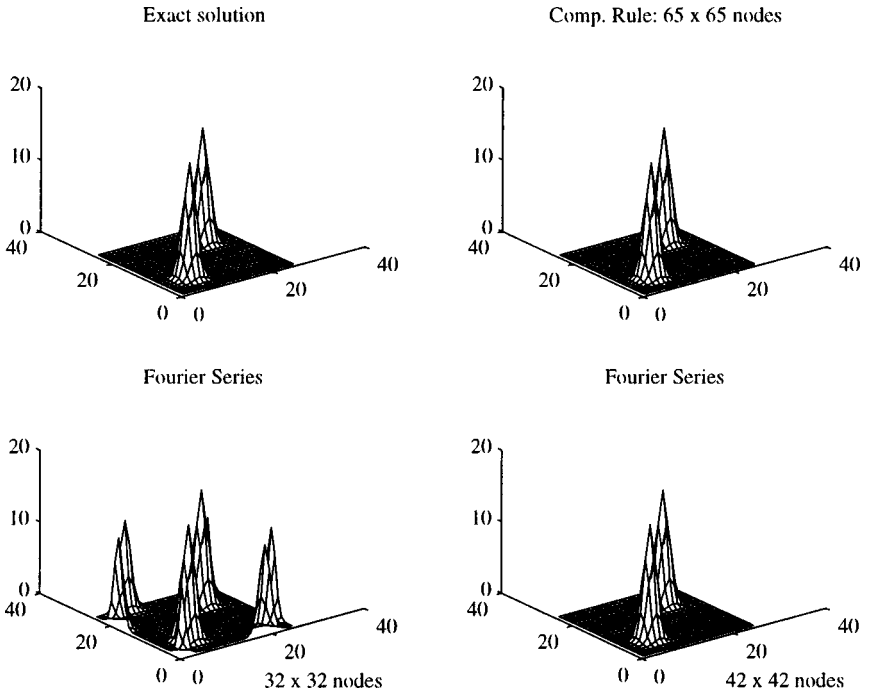

FIG. 3. Reconstruction of two Gaussian pulses (Example *2.2*) at $t = 0.005$. The upper right-hand plot uses a tensor product discretization based on our composite quadrature rule (26). The two lower figures show an underresolved Fourier discretization (left) and a resolved one (right). The number of nodes in both tight-hand figures is sufficient to guarantee six-digit accuracy.

The Fourier series requires approximately 10^6 modes to resolve the function, whereas the composite rule requires less than 6000 modes.

3. THE FAST ALGORITHM

Let us recall that the integral equation (10) to be solved takes the form

$$\frac{1}{2}\mu(\mathbf{x}, t) - D_L\mu(\mathbf{x}, t) = U_H(\mathbf{x}, t) - g(\mathbf{x}, t)$$

and that all of the nonlocal information is contained in

$$U_H(\mathbf{x}, t) = Vf(\mathbf{x}, t) + D_H\mu(\mathbf{x}, t).$$

To pose a concrete computational problem, we consider a discrete version of this evolution process in two dimensions. We assume that the initial data $f(\mathbf{y})$ is supported in $[0, \pi]^2$ and given on a square $m_1 \times m_1$ grid with mesh spacing $h = \pi/m_1$ and

$$f_{j,k} = f(jh, kh).$$

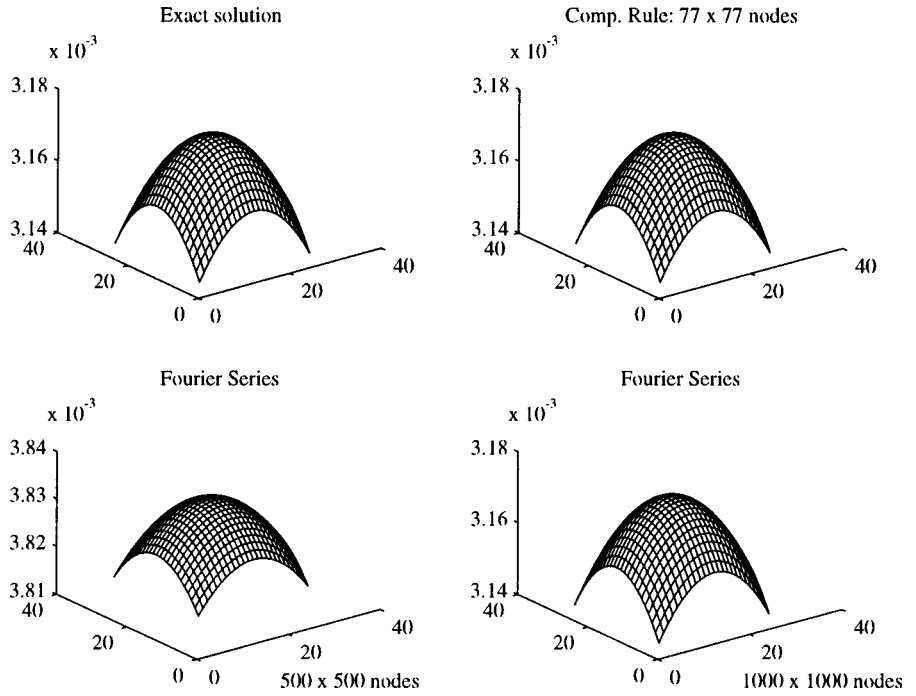

FIG. 4. Reconstruction of two Gaussian pulses (Example *2.2*) at $t = 50$. The upper right-hand plot uses a tensor product discretization based on our composite quadrature rule (26). The two lower figures show an underresolved Fourier discretization (left) and a resolved one (right). The number of nodes in both right-hand figures is sufficient to guarantee six-digit accuracy.

The boundary $\Gamma(t)$ is discretized at M points, equispaced in arclength

$$(\mathbf{b}_1(t), \mathbf{b}_2(t), \ldots, \mathbf{b}_M(t)),$$

with mesh spacing $h_b(t)$ and unit outward normal at $\mathbf{b}_m(t)$ given by $\mathbf{n}_m(t)$. We would like to compute the solution at N successive times $t_n = n\Delta t$. Note that, for the moment, δ and the number of Fourier modes, N_C, are free parameters. For the sake of simplicity, we set $\delta = \kappa\Delta t$, with κ a positive integer, and let

$$U_H(\mathbf{x}, t_n) = h^2 \sum_{j=1}^{m_1}\sum_{k=1}^{m_1} \frac{e^{\|\mathbf{x}-(jh,kh)\|^2/4t_n}}{4\pi t_n} f_{j,k} + \sum_{l=1}^{n-k} h_b(t_l) \sum_{m=1}^{M} \frac{\mathbf{n}_{m,l}\cdot(\mathbf{x}-\mathbf{b}_{m,l})}{2(t_n-t_l)} \frac{e^{-\|\mathbf{x}-\mathbf{b}_{m,l}\|^2/4(t_n-t_l)}}{4\pi(t_n-t_l)} \mu_m(l), \qquad (27)$$

for $n = \kappa + 1, \ldots, N$, where

$$\mathbf{n}_{m,l} = \mathbf{n}_m(t_l), \qquad \mathbf{b}_{m,l} = \mathbf{b}_m(t_l), \qquad \mu_m(l) = \mu(\mathbf{b}_{m,l}, t_l).$$

The cost of evaluating $U_H(\mathbf{b}_m(t_n), t_n)$ on the boundary alone is clearly of the order $O(N^2M^2 + NMm)$ where $m = m_1^2$. Using a fast algorithm, like the fast Gauss

transform [10], to accelerate the summation over the spatial variables would reduce the cost to $O(N^2M + N(M+m))$, which still grows quadratically with the number of time steps. A generalization of the fast Gauss transform introduced in [23] could be used to overcome this difficulty, but our approach follows that of [11].

Using the results of the previous section, we assume that the parameter N_C is chosen so that

$$\frac{e^{-(x_1^2+x_2^2)/4t}}{4\pi t} - \sum_{q=1}^{N_C}\sum_{r=1}^{N_C} w_q w_r e^{is_q x_1} e^{is_r x_2} e^{-s_q^2 t} e^{-s_r^2 t} = O(\epsilon). \tag{28}$$

Substituting this approximation into (27) yields the Fourier representation

$$U_H(\mathbf{x}, t_n) \approx \sum_{q=1}^{N_C}\sum_{r=1}^{N_C} C_{q,r}(n) e^{is_q x_1} e^{is_r x_2}, \tag{29}$$

where

$$\begin{aligned} C_{q,r}(n) = w_q w_r e^{-(s_q^2+s_r^2)t_n} \Bigg(& h^2 \sum_{j=1}^{m_1}\sum_{k=1}^{m_1} e^{-is_q j\pi/m_1} e^{-is_r k\pi/m_1} f_{j,k} \\ & + h_b(t_l) \sum_{l=1}^{n-\kappa} e^{(s_q^2+s_r^2)t_l} \sum_{m=1}^{M} (i\mathbf{s}_{q,r}\cdot\mathbf{n}_{m,l}) e^{-i\mathbf{s}_{q,r}\cdot\mathbf{b}_{m,l}} \mu_m(l) \Bigg), \end{aligned} \tag{30}$$

with $\mathbf{s}_{q,r} = (s_q, s_r)$.

At first glance, this looks worse than the original expression (27). Instead of dealing with one history-dependent function, we have N_C^2 of them! Upon closer inspection, however, it is evident that time plays a very different role in (30) than it does in the physical space description of U_H. In particular, the Fourier coefficients $C_{q,r}$ satisfy a simple recurrence relation,

$$C_{q,r}(n+1) = e^{-(s_q^2+s_r^2)\Delta t} C_{q,r}(n) + \mathcal{U}_{q,r}(n+1), \tag{31}$$

where

$$\mathcal{U}_{q,r}(n+1) = h_b(t_l) w_q w_r e^{-(s_q^2+s_r^2)\kappa\Delta t} \sum_{m=1}^{M} (i\mathbf{s}_{q,r}\cdot\mathbf{n}_m) e^{-i\mathbf{s}_{q,r}\cdot\mathbf{b}_m} \mu_m(n+1-\kappa). \tag{32}$$

In short, the Fourier modes are damped and updated at each time step, but the burden of history dependence is eliminated. For initialization, at $n = \kappa + 1$, we have

$$\begin{aligned} C_{q,r}(\kappa+1) = {} & h^2 w_q w_r e^{-(s_q^2+s_r^2)(\kappa+1)\Delta t} \sum_{j=1}^{m_1}\sum_{k=1}^{m_1} e^{-is_q j\pi/m_1} e^{-is_r k\pi/m_1} f_{j,k} \\ & + \mathcal{U}_{q,r}(\kappa+1). \end{aligned} \tag{33}$$

The double summation in (33) is clearly a kind of discrete Fourier transform. Since the spectral locations (s_q, s_r) are not equispaced, however, the classical FFT does not apply. Fortunately, in the past few years, versions of the FFT have been constructed which do apply [2, 7, 22] and which require $m \log m + N_C^2$ work. We refer the reader to the cited papers for details. The summations over boundary points in computing the "updates" $\mathcal{U}_{q,r}$

in (32) are also discrete Fourier transforms evaluated at nonequispaced points, but with a singular source distribution. The nonequispaced FFT can be used for this step as well, requiring $O(M \log M + N_C^2)$ work.

We are now in a position to fix values for the parameters N_C and δ. Since we would like to limit the work per time step to $O(M \log M)$, it is sufficient to choose $p = \sqrt{M}$, so that $N_C = O(p)$ and $N_C^2 = O(M)$. It remains only to choose δ. Recall now, from Lemma 2.2, that the error in truncating the Fourier integral at the frequency $|s| = p$ is of the order

$$\frac{e^{-p^2\delta}}{4\pi\delta}.$$

With $p = \sqrt{M}$ already defined, choosing $\delta = \kappa \log M/M$ yields an error of the order

$$\frac{e^{-p^2\delta}}{4\pi\delta} = \frac{e^{-\kappa \log M}}{4\pi\kappa \log M} M = o\left(\frac{1}{M^{\kappa-1}}\right).$$

For the sake of simplicity, we choose the time step $\Delta t = \log M/M$. The preceding discussion then proves the following result: for any prescribed order of accuracy, the entire history of the evolution process, up to the last few time steps, can be encompassed in a Fourier representation using only $O(M)$ modes.

We have ignored the calculation of the local part, but both asymptotic and direct numerical approaches to the evaluation of D_L in (9) require an amount of work proportional to κM. Since κ is a fixed integer for a fixed order of accuracy, we are done. The total amount of work required is of the order

$$O(m \log m + NM \log M + \kappa M).$$

The first term stems from computing the Fourier transform of the initial data, the second from the evaluation of U_H, and the third from the local part D_L.

4. CONCLUSIONS

We have presented a new discrete spectral approximation of the free space heat kernel, which results in an extremely efficient representation of diffusion processes over long time intervals. The method developed here may be of use in other problems with continuous spectra.

To be incorporated into a solver for exterior heat equations, a significant amount of work is still required. This includes adaptation of the nonequispaced FFT, the development of accurate quadrature rules for the local part, etc. A full implementation will be described in a forthcoming paper.

REFERENCES

1. M. Abramowitz and I. Stegun, Eds., "Handbook of Mathematical Functions," Dover, New York, 1965.
2. G. Beylkin, On the fast Fourier transform of functions with singularities, *Appl. Comput. Harmon. Anal.* **2** (1995), 363–381.

3. K. Brattkus and D. I. Meiron, Numerical simulations of unsteady crystal growth, *SIAM J. Appl. Math.* **52** (1992), 1303–1320.
4. C. A. Brebbia, Ed., "Topics in Boundary Element Research," Vol. 1, Springer-Verlag, Berlin, 1981.
5. R. Brown, "Layer Potentials and Boundary Value problems for the Heat Equation on Lipschitz Cylinders," Ph.D. Thesis, University of Minnesota, 1987.
6. P. J. Davis and P. Rabinowitz, "Methods of Numerical Integration," Ginn, Blaisdell/Boston, 1967.
7. A. Dutt and V. Rokhlin, On the rapid evaluation of trigonometric series, Research Report 893, Yale Computer Science Department, 1992.
8. H. P. Dym and H. P. McKean, "Fourier Series and Integrals," Academic Press, San Diego, 1972.
9. A. Friedman, "Partial Differential Equations of Parabolic Type," Prentice-Hall, Englewood Cliffs, NJ, 1964.
10. L. Greengard and J. Strain, The fast Gauss transform, *SIAM J. Sci. Stat. Comput.* **12** (1991), 79–94.
11. L. Greengard and J. Strain, The fast algorithm for the evaluation of heat potentials, *Comm. Pure Appl. Math.* **43** (1990), 949–963.
12. R. B. Guenther and J. W. Lee, "Partial Differential Equations of Mathematical Physics and Integral Equations," Prentice-Hall, Englewood Cliffs, NJ, 1988.
13. E. Hill, A class of reciprocal functions, *Ann. of Math.* **27** (1926), 427–464.
14. P. D. Koumoutsakos, "Direct Numerical Simulations of Unsteady Separated Flows Using Vortex Methods," Ph.D. Thesis, California Institute of Technology, 1993.
15. P. Lin, "On the Numerical Solution of the Heat Equation in Unbounded Domains," Ph.D. Thesis, New York University, 1993.
16. A. McIntyre, Boundary integral solutions of the heat equation, *Math. Comp.* **46** (1986), 71–79.
17. S. G. Mikhlin, "Integral Equations," Pergamon Press, New York, 1957.
18. L. Morino and R. Piva, Eds., "Boundary Integral Methods: Theory and Applications," Springer-Verlag, Berlin, 1990.
19. P. J. Noon, "The Single Layer Heat Potential and Galerkin Boundary Element Methods for the Heat Equation," Ph.D. Thesis, University of Maryland, 1988.
20. W. Pogorzelski, "Integral Equations and Their Applications," Pergamon Press, Oxford, 1966.
21. J. A. Sethian and J. Strain, Crystal growth and dendritic solidification, *J. Comput. Phys.* **98** (1992), 231–253.
22. J. Strain, Fast potential theory II. Layer potentials and discrete sums, *J. Comput. Phys.* **99** (1992), 251–270.
23. J. Strain, Fast adaptive methods for the free-space heat equation, *SIAM J. Sci. Comput.* **15** (1992), 185–206.